Fault Ride-Through of Large Wind Farms Using Series Dynamic Braking Resistors (March 2007)

Andrew Causebrook, David J. Atkinson, and Alan G. Jack, *Member, IEEE*

***Abstract*—Fault ride-through (FRT) is required for large wind farms in most power systems. Fixed speed wind turbines (FSWTs) are a diminishing but significant sector in the fast-growing wind turbine (WT) market. State-of-art techniques applied to meet grid requirements for FSWT wind farms are blade pitching and dynamic reactive power compensation (RPC). Blade pitching is constrained by the onerous mechanical loads imposed on a wind turbine during rapid power restoration. Dynamic RPC is constrained by its high capital cost. These present technologies can therefore be limiting, especially when connecting to smaller power systems. A novel alternative technology is proposed that inserts series resistance into the generation circuit. The series dynamic braking resistor (SDBR) dissipates active power and boosts generator voltage, potentially displacing the need for pitch control and dynamic RPC. This paper uses a representative wind farm model to study the beneficial effect of SDBR compared to dynamic RPC. This is achieved by quasi-steady-state characterization and transient FRT stability simulations. The analysis shows that SDBR can substantially improve the FRT performance of a FSWT wind farm. It also shows that a small resistance, inserted for less than one second, can displace a substantial capacity of dynamic RPC.**

***Index Terms*—Dynamic braking resistors, fault ride-through, wind farm stability, wind turbine generators.**

I. Introduction

FAULT ride-through (FRT) is now required for connection of large wind farms in most power systems. The FRT-compliant wind farm must remain connected and actively contribute to system stability during a wide range of network fault scenarios. FRT is particularly important in securing stability in regions where wind is becoming a significant contributor to the power system's dynamic performance.

FRT performance requirements differ according to the dynamic characteristics of the power system concerned. Smaller power systems, with little or no interconnection, are more prone to frequency instability, and hence, their Codes typically emphasize the provision of active power. Ireland, with a maximum system demand of 6 GW, represents a small, near-isolated national system with a challenging requirement to restore power within one second of fault clearance [1], [2]. Great Britain, with a maximum demand of 60 GW, represents a larger near-isolated system with similar requirements [3], [4]. In contrast, frequency stability in continental European countries such as Germany is strengthened by interconnections within the Union for the Co-operation of Transmission of Electricity (UCTE). UCTE members therefore have less onerous power restoration requirements [5], [6].

TABLE I
Wind Technology Enhancements to Meet FRT Challenge

Type	FRT enhancement
A.	Dynamic reactive power compensation (RPC)
B.	As above + pitch control
C.	Rotor converter protection + pitch control
D.	Pitch control + braking resistors on dc link

The wind industry has responded to the introduction of FRT requirements in several ways according to wind turbine technology type. For the purpose of considering FRT response, it is convenient to categorize commercial wind turbines in four main types [7], [8]:

A) fixed-speed wind turbines (FSWTs) with fixed pitch;
B) FSWTs with variable pitch (active stall);
C) variable-speed wind turbines (VSWTs) with doubly-fed induction generators (DFIGs);
D) VSWTs with fully-rated converters.

Type A WTs were dominant in the 1990s but now retain less than 1% of the world market share. Type B WTs have retained a sizeable market share and have accumulated an installed world capacity of approaching 10 GW. Type C has been the dominant technology since about 2002, but type D may challenge this dominance in the future as the cost of power electronics continues to fall. Specific technical developments made in response to FRT requirements are summarized in Table I.

Pitch control is therefore a central feature of most FRT strategies for modern wind turbines. However, there are still significant response limitations when this method is applied to smaller power systems. Although the blade pitch actuators are powerful enough to fully pitch the blades within a fraction of a second, the dynamic forces resulting from restoring power at this rate are very onerous. Faster restoration times may be achieved by improved structural design, but it is likely that these dynamic forces will remain a substantial design issue where sub-second restoration times are required. As a consequence, pitch control is not the final solution for FRT compliance, and there is still an opportunity for technologies that reduce or eliminate dependence on pitch control systems or allow retrospective enhancement of existing wind farms. This paper proposes series dynamic braking resistors (SDBRs) as a promising alternative, with particular applicability to FSWTs (types A and B) and possible extension to other generation technologies. The SDBR concept was introduced by the authors in 2005-2006 [9], [10]. The purpose of this paper is to present detailed analysis and transient simulation results of its performance and assess its beneficial effects compared to state-of-art alternatives.

Manuscript received September 6, 2006; revised March 13, 2007. This work was supported in part by the New and Renewable Energy Centre (NaREC) and in part by an EPRSC studentship. Paper no. TPWRS-00624-2006.

The authors are with the Electrical Machines and Drives Group, Newcastle University, Newcastle-upon-Tyne, U.K. (e-mail: Andrew.Causebrook@newcastle.ac.uk).

Digital Object Identifier 10.1109/TPWRS.2007.901658

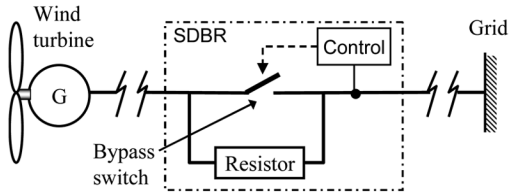

Fig. 1. SBDR schematic arrangement.

II. SDBR Concept

The SDBR concept aims to contribute directly to the balance of active power during a fault, thus displacing or eliminating the need for pitch control. It does this by dynamically inserting a resistor in the generation circuit, increasing the voltage at the terminals of the generator and thereby mitigating the destabilizing depression of electrical torque and power during the fault period.

The general schematic arrangement of SDBR is shown in Fig. 1.

SDBR is shown located between the wind turbine(s) and the grid in Fig. 1. The actual position of the device within a particular wind farm topology will depend on the space available to install it and the relative cost of switching at low, medium, and high voltage. The bypass switch could be mechanical, allowing multi-cycle response and discrete control, or static, allowing sub-cycle response and smoothly variable control. This paper focuses on single-stage mechanical switching as the lowest cost and least complex option with potential to strongly contribute to FRT compliance of FSWTs.

SDBR would operate with its switch closed under normal conditions, bypassing the braking resistor. Voltage depression below a selected set-point would lead to near-instantaneous tripping of the switch. Current would then flow through the inserted resistor for the period of the fault and the initial post-fault recovery. When voltage recovered above a minimum reference level, the switch would close and the circuit would be restored to its normal state. During the short insertion period, the energy would be dissipated in the resistor, raising its temperature. The resistor would be selected according to the limiting temperature of its resistive elements and the maximum energy dissipated during the insertion period.

Previous DBR topologies proposed by Wu [11] and Freitus [12] for wind farm stability have a shunt-connected topology, in the manner previously applied to improve transmission and synchronous generator stability [13], [14]. The distinctive advantage of series-SDBR over shunt-DBR is derived from the fact that its effect is related to *current* magnitude rather than *voltage* magnitude. SDBR is therefore most effective during the combined high generation, low residual voltage conditions that are most onerous for FRT. The effect is shown schematically in Fig. 2.

Fig. 2 shows how generated power is transferred across the wind farm system, while excess dynamic power is stored in its drive train and heat is dissipated by SDBR. The effect on stator voltage is illustrated by the phasor diagram of Fig. 3.

It can be seen from Fig. 3 that stator voltage, v_s, is increased in magnitude by the voltage, iR_{sdbr}, across SDBR. Since mechanical torque is proportional to the square of the stator voltage of an induction machine, it can be inferred that the presence of SDBR will increase the mechanical power extracted from the drive train and therefore reduce its speed excursion during a voltage dip. This effect would improve the post-fault recovery of a wind farm system. Fig. 3 also shows the limiting beneficial case (dotted phasors) at very low power factor when SDBR has no effect on stator voltage magnitude.

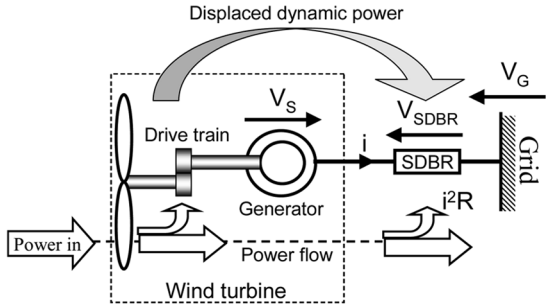

Fig. 2. Conceptual benefit of SBDR under fault conditions.

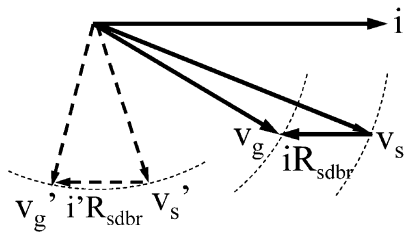

Fig. 3. Phasor diagram showing the effect of SDBR on stator voltage.

III. Methodology

Section II has introduced the SDBR concept and provided a theoretical basis for its application to FRT. Simulation and analysis are required to support this theoretical assertion and establish the magnitude and the extent of its beneficial effect compared to state-of-art dynamic RPC. This section previews the methodology used in this paper to achieve this objective.

The first step in Section IV is to establish a reduced FSWT (type A or B) system that is representative of a large modern wind farm. This representative wind farm system is then characterized by steady-state analysis in Section V to illustrate the effect of SDBR over a range of super-synchronous rotor speeds. The validity and limitation of using steady-state analysis to infer FRT performance benefits is examined. A transient model of the representative wind farm system is then presented in Section VI and used to simulate selected fault scenarios in order to verify the effect of SDBR. The dynamic response of a *one-mass* system is used to study underlying FRT characteristics and check the validity of inferring transient behavior from steady-state characteristics. The dynamic response of a *two-mass* system is then used to compare the performance of SDBR with dynamic RPC. Finally, the same transient model is used to check the effectiveness of SDBR and dynamic RPC during a prolonged phase-to-phase grid fault.

Simulation results are used to draw conclusions regarding the strength and extent of the potential FRT application of SDBR with FSWT-wind farms.

IV. Representative Wind Farm System

There is a broad range of practical wind turbine and wind farm configurations. The purpose of this section is to define a

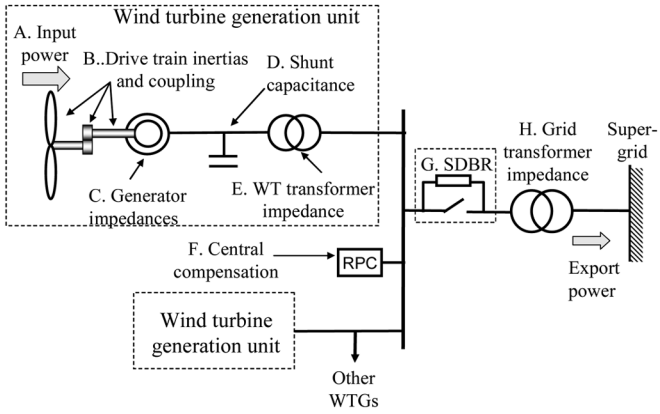

Fig. 4. Typical large wind farm single line diagram.

single representative wind farm system for all for the steady-state and transient analyses presented in this paper.

A typical large wind farm comprising multi-megawatt FSWTs and incorporating SDBR is represented by the single line diagram of Fig. 4.

Fig. 4 annotates the key parameters that influence stability of the system associated with a supergrid fault. These parameters are quantified and discussed below. All quantities are given in per unit form using wind turbine or wind farm active power rating as the power base.

A. Mechanical Power Input

Wind turbine input power is highly variable and unsteady, resulting in large and rapid variations in power transfer [15, pp. 135–136]. For the purpose of studying worst-case FRT performance, these variations detract from observation of the fundamental system dynamics. Furthermore, they are smoothed over a wind farm with a large number of WTs because of their non-coherence. An equivalent constant power input has therefore been used in this paper [16, p. 532]. Since maximum generation conditions are worst-case for FRT assessment, an *input power of 1.05 p.u.* has been chosen to account for a realistic one-second overpower condition for a large wind farm.

B. Drive Train Inertia and Coupling

Drive train inertia is highly influential in the dynamic performance of a wind farm system. Lumped inertia constants (H) for WTs are typically in the range 2.4–6.8 s [16, p. 545]. Data from commercial 1.3-MW WTs suggest that 4.5 s is a representative value for this study.

Drive train coupling is highly significant. It is now generally accepted that two-mass representation of a WT drive train is a necessary feature for dynamic analysis [17]. Data from a selection of multi-megawatt WTs suggest that a low speed to high speed inertia ratio of six to eight and an eigenfrequency of 2 Hz are broadly representative values. Mechanical friction and damping have little effect on system stability and are neglected. In summary, the following drive train parameters are used in this paper:

$$\begin{aligned} \text{Low speed inertia constant}: &\quad H_{\rm ls} = 4\,\text{s} \\ \text{High speed inertia constant}: &\quad H_{\rm hs} = 0.5\,\text{s} \\ \text{Eigenfrequency (free-free)}: &\quad f_{\rm eig} = 2\,\text{Hz}. \end{aligned}$$

C. Induction Generator Impedances

Induction generator impedances are highly influential on the wind farm's FRT performance. Efficient multi-megawatt machines must have low rotor resistance and therefore a steep torque-slip curve at rated power and a low "pull-away" slip. The FRT response of a wind farm is particularly sensitive to rotor resistance, and therefore, the selected value of *0.007 p.u.* on WT rating is carefully chosen with reference to real WT data. Saturation effects, core losses, and the slip-dependence of impedance magnitudes are not accounted for in this study.

The following generator impedances have been used for all studies in this paper:

$$\begin{aligned} \text{Stator resistance}: &\quad R_s = 0.006\,\text{p.u.} \\ \text{Stator leakage inductance}: &\quad L_{\rm sl} = 0.14\,\text{p.u.} \\ \text{Rotor resistance}: &\quad R_r = 0.007\,\text{p.u.} \\ \text{Rotor leakage inductance}: &\quad L_{\rm rl} = 0.05\,\text{p.u.} \\ \text{Magnetizing inductance}: &\quad L_m = 3.0\,\text{p.u.} \end{aligned}$$

D. Shunt Capacitance (Local to WT)

WT shunt capacitance traditionally comprises fixed no-load and switched load compensation banks. Grid codes now impose steady-state reactive power *export* requirements and transient voltage control requirements that demand further provision met locally or centrally (see Subsection F). The base-case for the studies in this paper is *reactive power compensation* (RPC) *of 1.0 p.u. using shunt capacitors*, capable of meeting typical steady-state grid requirements. These capacitors are assumed to be connected throughout the FRT simulations. Additional dynamic RPC is used only for comparison with SDBR.

E. WT Transformer Impedance

Wind farms have dedicated step-up WT transformers. Typically multi-megawatt WT transformers have lumped series reactance of 0.06 p.u. and resistance of 0.01 p.u. The transformers are modeled as series impedance in steady state and transient analysis in this paper.

F. Central Reactive Power

Central RPC can be provided by switched capacitors, SVC [18] or STATCOM [19]. Central RPC has a marginally different effect on FRT performance than local RPC due to the interposing turbine transformers and cabling. However, for the purpose of these generic studies, central RPC has been omitted in order to allow the lumping of wind farm and grid impedance (see Subsection I).

G. SDBR

SDBR can be located centrally or distributed at each turbine transformer. Central location is advantageous where there are large numbers of WTs because a single device can be installed at the site substation, avoiding the space and/or planning constraints at the turbine tower. Although there is some difference in the FRT performance of these two options, the distributed SDBR option has been used in these studies to reduce the complexity of the wind farm equivalent (see Subsection I) and the transient model. The distributed SDBR is switched by

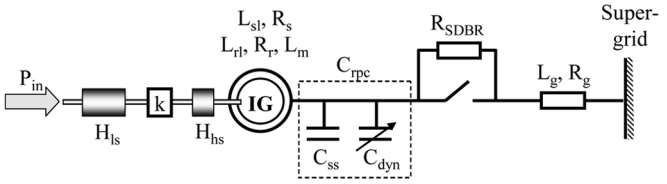

Fig. 5. Reduced schematic of representative wind farm.

a fast-acting bypass contactor triggered by an instantaneous undervoltage relay. The total insertion time for such an arrangement would be about 40 ms. In the base case studies, the resistor is switched out after one second in order to limit thermal loading on the resistor and avoid unnecessary dissipation of power after recovery.

H. Grid Transformer Impedance

The grid transformer is an important component of a large wind farm system because of its substantial impedance. A dedicated step-up transformer with a lumped series reactance of 0.10 p.u. and resistance of 0.05 p.u. is selected as representative for a large wind farm.

I. Equivalent Representation

Having defined parameters for each major component of a representative wind farm system, a reduced equivalent can be derived for the purpose of steady-state and transient analysis. The first reduction is the lumping of multiple WT units into a single equivalent with rating equal to the sum of the individual units and per unit values equal to those of the individual units. This is justified by the fact that identical power inputs and system parameters have been used for each WT unit. The second reduction is the lumping of WT and grid transformers and miscellaneous grid impedance as a single series impedance neglecting shunt capacitance and transformer magnetizsing reactance. Omission of transformer inrush is not highly significant for the comparative assessment of this paper. The following lumped values are therefore proposed for this study:

$$\text{Grid resistance}: \quad R_g = 0.04\,\text{p.u.}$$
$$\text{Grid inductance}: \quad L_g = 0.20\,\text{p.u.}$$

In summary, the reduced, representative model carried forward for analysis in the following sections is shown in Fig. 5.

V. Steady-State Characterization

A. Introduction

The purpose of this section is to characterize the influence of SDBR on steady-state wind farm power flows and thereby infer potential FRT enhancements of the representative wind farm system of Fig. 5. Two enhancement technologies are compared: state-of-art dynamic RPC and SDBR. However, before proceeding with this analysis, it is important to relate the time frames of fault events and system time constants. The range of applicable grid faults is defined by the voltage-duration profile of Fig. 6(a) and illustrated by the selected fault scenarios of Fig. 6(b).

Fig. 6(a) is taken from the GB Grid Code [CC.A.4.3, 4] but is of a form typical of the requirements of many modern grid codes. The profile does not describe a single fault event but the envelope of rectangular voltage notches associated with worst-case grid faults. The ac time constant, $\mathrm{T_{ac}}$, for system transients is derived from the following equation:

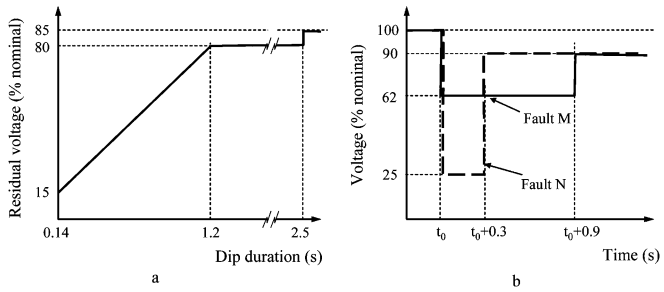

Fig. 6. Voltage-duration profiles for grid voltage dips. (a) Grid voltage-duration profile. (b) Selected grid fault scenarios.

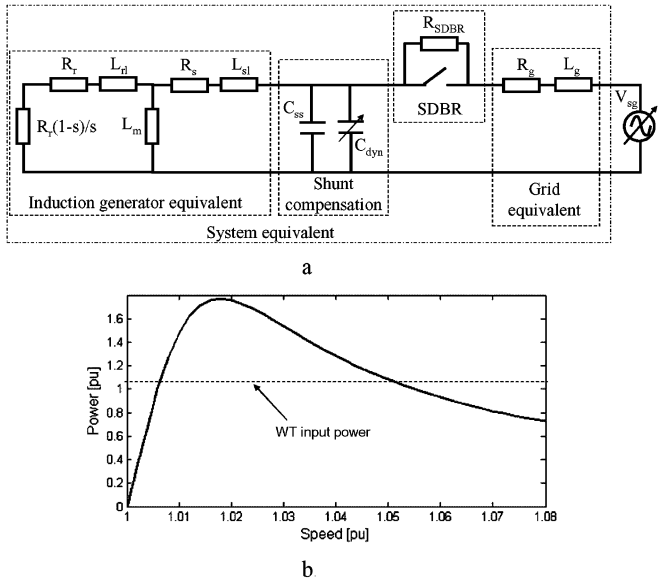

Fig. 7. Equivalent circuit and power curve for representative wind farm. (a) Equivalent circuit. (b) Decelerating power versus speed characteristic (rated grid voltage).

$$\mathrm{T_{ac}} = \frac{\mathrm{X_T}}{\omega \mathrm{R_r}} \tag{1}$$

where

$$X_T = \text{system Thevenin equivalent reactance}(\Omega);$$
$$\omega = \text{system angular frequency}(\mathrm{rad}s^{-1}).$$

The time constant is calculated to be 180 ms for the system equivalent of Fig. 7 and noted to be independent of stator resistance. The two voltage-time traces shown in Fig. 6(b) are used to represent faults with long and short time durations relative to this time constant. The long duration fault, M, can be approximated as three steady-state conditions. The short duration fault, N, will be heavily influenced by the system transient response, and steady-state characteristics are less directly indicative of stability in this case (see Section V-F2).

B. Steady-State Power Characterization

The single-phase, positive sequence circuit equivalent for the representative wind farm of Fig. 5 is shown in Fig. 7(a) with per unit slip, s.

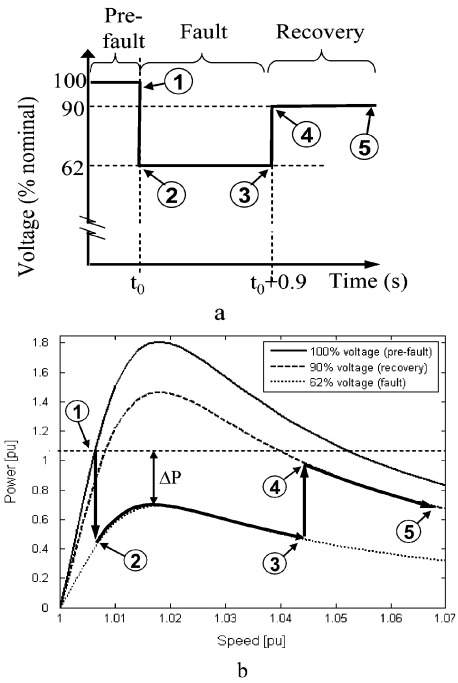

Fig. 8. Real-time power-speed trajectory. (a) Annotated fault scenario. (b) Power-speed trajectory.

The steady-state power transfer capability of an FSWT wind farm is characterized by the power-speed curves derived from the equivalent circuit of Fig. 7(a). There are two power characteristics of interest in FRT assessment: the decelerating power extracted from the mechanical system (determining the dynamic stability of the wind farm system) and the power exported to the grid (supporting the dynamic stability of the overall power system). This paper is concerned primarily with wind farm stability and therefore focuses on decelerating power characteristics, as shown in Fig. 7(b).

C. Quasi-Steady-State Assessment

Having introduced the steady-state power-speed characteristics of the wind farm system, the next step is to consider drive train dynamics within each period of the fault and plot the resulting real-time trajectory onto quasi-steady-state characteristics. In order to emphasize the effect of FRT enhancement techniques, a low lumped inertia constant of 2.5 s has been used for the following assessment. Furthermore, the effects of electrical system transients have been neglected at this stage. The resulting quasi-steady-state analysis is illustrated by Fig. 8 for the base-case wind farm system.

Fig. 8(a) shows the voltage-time characteristic of fault M. Fig. 8(b) shows the dynamic trajectory of the system superimposed onto the steady-state power-speed curves for each of the voltage levels associated with the fault. The key determinant of stability is acceleration during the fault period (driven by the net accelerating power, ΔP) and the power balance at fault clearance. In Fig. 8(b), the input power is greater than the decelerating power at this time, and therefore, the system is unstable. The primary objective of FRT enhancing technologies is therefore to improve the balance of power at this crucial point.

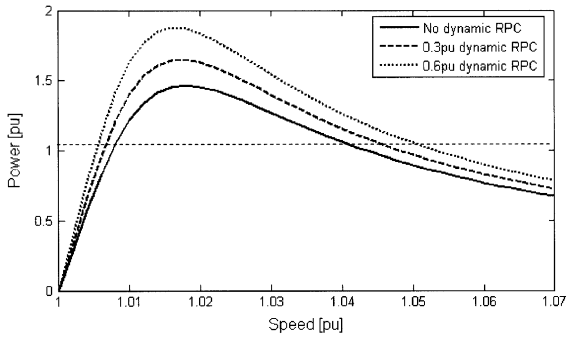

Fig. 9. Effect of dynamic RPC on steady-state characteristics.

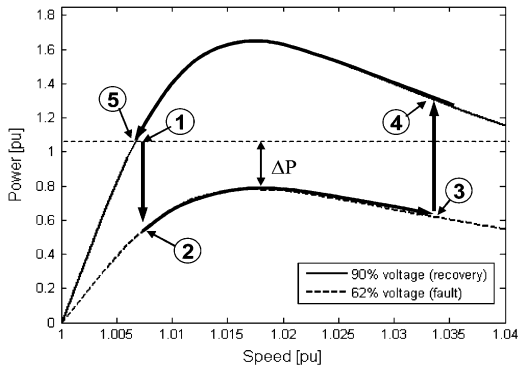

Fig. 10. Enhanced FRT response with dynamic RPC.

D. Improving Stability Using Dynamic RPC

The state-of-art method for enhancing FRT performance of wind farms comprising FSWTs is to insert dynamic RPC, using thyristor-switched capacitors, SVC or STATCOM. The effect of thyristor-switched capacitors on the steady-state system power characteristics is shown in Fig. 9.

Fig. 9 shows the effect of 0.3- and 0.6-p.u. dynamic RPC on the steady-state power characteristics with 90% grid recovery voltage. It can be observed that the dynamic RPC lifts the power characteristic throughout the speed range by about 15% for each 0.3-p.u. RPC increment.

The effect of 0.3-p.u. dynamic RPC on the quasi-steady-state response of the wind farm to fault M is shown in Fig. 10.

It can be observed that the net accelerating power, ΔP, is less than the base-case study in Fig. 8(b), resulting in reduced speed excursion at fault clearance (3). Furthermore, the recovery characteristic is greater in magnitude, resulting in a significant net decelerating power in the recovery phase. The combination of these factors means that the enhanced system has a good margin of stability.

E. Improving Stability Using SDBR

The effect of SDBR on the steady-state system power characteristics is shown in Fig. 11.

Fig. 11 shows the effect of 0.05- and 0.1-p.u. SDBR on the steady-state power characteristics with 90% grid recovery voltage. It can be observed that the peak power is increased substantially (about 40% for 0.1-p.u. SDBR), but the improvement in the power characteristic diminishes substantially with increasing speed. This qualitative effect was predicted from the phasor diagram of Fig. 3.

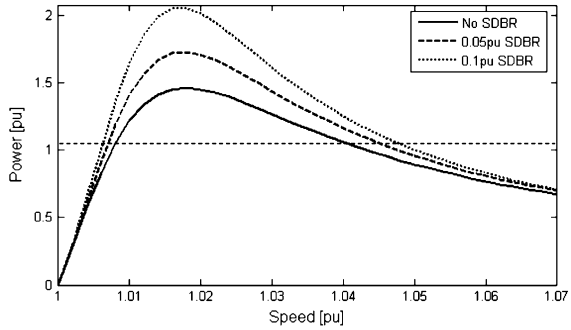

Fig. 11. Effect of dynamic SDBR on steady-state characteristics.

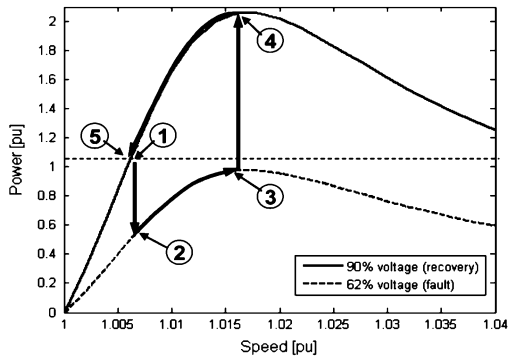

Fig. 12. Enhanced FRT response with SDBR.

The effect of 0.1-p.u. SDBR on the quasi-steady-state response of the wind farm to fault M is shown in Fig. 12.

It can be observed that the net accelerating power, ΔP, tends to zero during the fault period so that a quasi-stable position is reached at the residual voltage level. When the fault is cleared, a large decelerating power is applied (point 4), rapidly restoring the system to near-nominal speed. The enhanced system therefore has a very large margin of stability.

F. Effect of System Transients

The influence of system transients on quasi-steady-state assessment becomes progressively more significant for faults of shorter duration. These influences are conveniently categorized as *dynamical*, arising from generator rotor acceleration or deceleration, and *transient*, arising from electrical voltage steps. The following analysis seeks to examine each influence in isolation using the full transient model described in Section VI.

1) Dynamical Influence: Acceleration (α) scenarios of 0.3 p.u. and -0.15 p.u. have been selected to represent the higher end of likely acceleration magnitudes arising from two-mass simulations (i.e., Fig. 18). The acceleration and deceleration simulations, with and without SDBR, were initialized at 1.0-p.u. and 1.1-p.u. speeds, respectively. Fig. 13 shows the results of these simulations.

Fig. 13 shows that acceleration "shears" the power-speed curves in the direction of higher speed and power magnitude, and deceleration "shears" the power-speed curves in the direction of lower speeds and power magnitude. The key observation for the purpose of this qualitative assessment is that the beneficial effect of SDBR is sustained in each case.

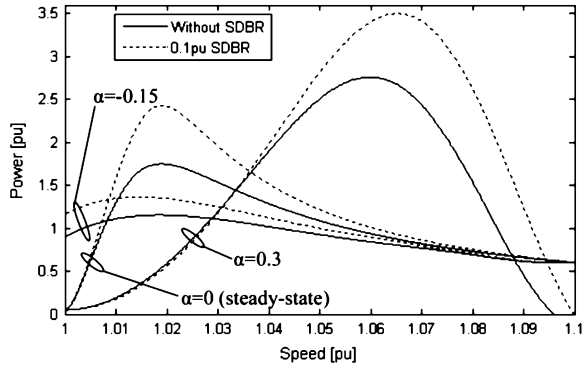

Fig. 13. Effect of acceleration on steady-state wind farm power characteristic.

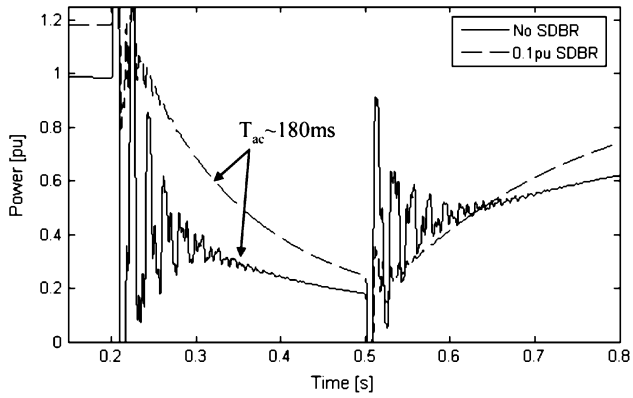

Fig. 14. Transition of mechanical power during fault N.

2) Transient Influence: Fig. 14 shows the transition of mechanical power associated with the voltage steps of fault N in Fig. 6 with speed constrained to nominal.

It can be observed that SDBR does not change the voltage decay time constant [$\sim$180 ms, as derived from (1)]. but it does substantially increase the initial mechanical power exported into the electrical system during the fault. It is also evident that SDBR strongly damps the dc-induced 50-Hz oscillating component of power in the period after each voltage transition.

After fault clearance, the power export with SDBR is initially depressed but rises quickly to exceed the base-case.

VI. Transient Simulation of Wind Farm System

A. Introduction

The benefits of SDBR and dynamic RPC have been inferred from steady-state analysis in Section V. This section introduces a transient model of the wind farm system and applies it in Matlab-Simulink to confirm these inferred benefits in comparison to dynamic RPC for balanced and unbalanced FRT simulations. The transient model is shown in the schematic diagram of Fig. 15.

Fig. 15 corresponds directly to the single line diagram in Fig. 5 with each transfer function, G(s), relating to a system component. G(s) has the general form of

$$\mathrm{G(s)} = \frac{\mathrm{b(s)}}{\mathrm{a(s)}} = \frac{1}{\mathrm{Xs} + \mathrm{Y}} \tag{2}$$

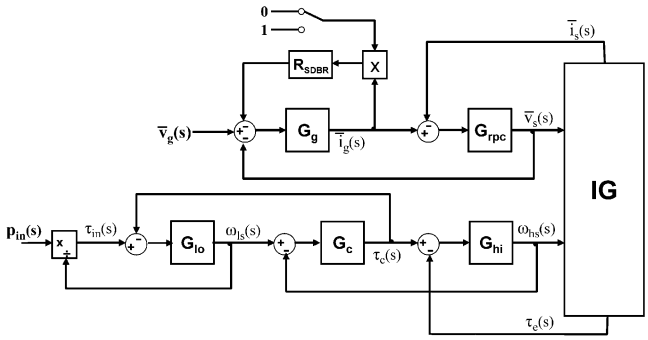

Fig. 15. Schematic diagram of transient model with single mass.

TABLE II
SYSTEM PARAMETERS

Component	Function	X	Y
Mechanical system:			
Low-speed inertia	$G_{ls}(s)$	$2H_{ls}$	0
Shaft coupling	$G_c(s)$	K_c	10^3
High-speed inertia	$G_{hs}(s)$	$2H_{hs}$	0
Electrical system:			
Grid impedance	$G_g(s)$	L/ω_0	R_g
Reactive power comp.	$G_{rpc}(s)$	C_{rpc}/ω_0	10^3
Notes: B_c *&* R_{rpc} *are inserted for numerical stability only* $C_{rpc}=C_{ss}+kC_{dyn}$, *where k is 1 during the fault and ramps to zero during the recovery period (no proportional control)*			

where

$a(s)$ and $b(s)$ are input and output functions, respectively :

scalar functions for mechanical system

space vector functions for electrical system

X and Y are inertia (inductance) and damping (resistance).

X and Y are referenced to physical parameters in Table II.

Typical values from Section IV are assigned to each parameter in the transient studies presented in this section. The induction generator block, IG, represents a transfer function derived from

$$\bar{v}_s = R_s\bar{i}_s + \frac{1}{\omega_0}\frac{d\bar{\lambda}_s}{dt} \tag{3}$$

$$\bar{v}_r = R_r\bar{i}_r + \frac{1}{\omega_0}\frac{d\bar{\lambda}_r}{dt} - \omega_r M\bar{\lambda}_r = 0 \tag{4}$$

where

M is $\pi/2$ rotation operator

$\bar{v}_s$ and $\bar{v}_r$ are p.u. stator and rotor space vector voltages

$\bar{i}_s$ and $\bar{i}_r$ are p.u. stator and rotor space vector currents

ω_0 and ω_r are base speed (rad/s) and p.u. rotor speed

$\bar{\lambda}_s = L_m\bar{i}_r + L_{sl}\bar{i}_s$ is p.u. stator space vector flux linkage

$\bar{\lambda}_r = L_m\bar{i}_s + L_{rl}\bar{i}_r$ is p.u. rotor space vector flux linkage.

B. Balanced Lumped Mass Simulation

The purpose of this lumped mass simulation is to establish the underlying transient effect of SDBR with minimum complexity.

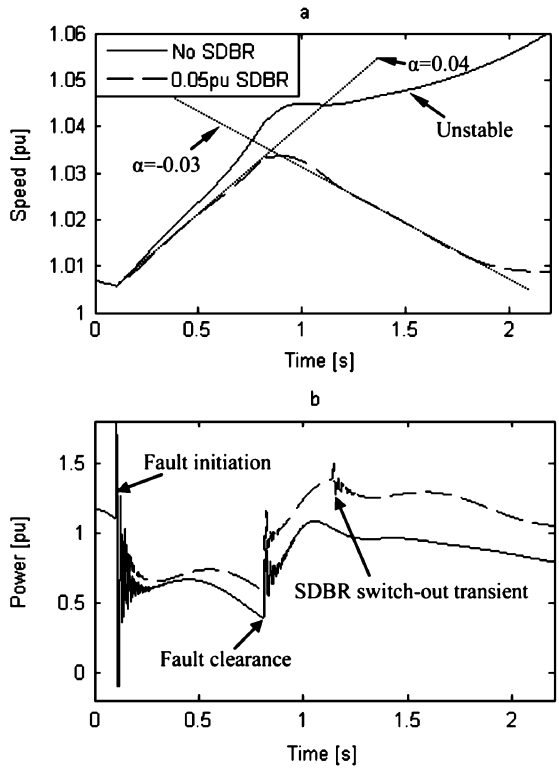

Fig. 16. Effect of SDBR on wind farm FRT performance.

The model of Fig. 15 is reduced by lumping high and low speed inertias to form a single drive train inertia constant, H, of 4.5 s.

The fault scenario selected for this example is 710 ms at 50% residual voltage, and 0.05 pu SDBR was selected as the minimum value that safely allowed recovery of the system for all fault scenarios derived from the voltage-duration profile of Fig. 6. The results of this scenario, simulated using the model of Fig. 15, are shown in Fig. 16.

Fig. 16(a) shows that SDBR transforms an unstable condition into a comfortably stable one. The reason for this improvement is illustrated by Fig. 16(b), which shows the increase in mechanical power extracted from the drive train both during and after the fault. This beneficial effect is repeated for the full range of faults described by the voltage duration profile of Fig. 6 and makes the difference between stability and instability in the fault duration range of 500–800 ms. Fig. 17 shows the correlation between the transient simulation results and those predicted from quasi-steady-state analysis with reference to the plot of rotor's power-speed FRT trajectory.

The FRT trajectory of the rotor in Fig. 17 starts at the system's pre-fault operating point (1.006, 1.05), accelerates up to the instant of fault clearance (1.033, 0.6), and then decelerates to its post-fault operating point (1.007, 1.05). The dynamically-adjusted steady-state characteristics associated with the fault ($\alpha = 0.04$ p.u.) and recovery ($\alpha = -0.03$ p.u.) are superimposed onto the power-speed plot. It can be observed that the FRT trajectory converges with these characteristics in both cases following an initial voltage transient error, as predicted in Section V-F.

C. Balanced Two-Mass Simulation

Having established the reduced wind farm's underlying FRT response and correlated it with quasi-steady-state analysis, this section compares the performance and sensitivities of SDBR

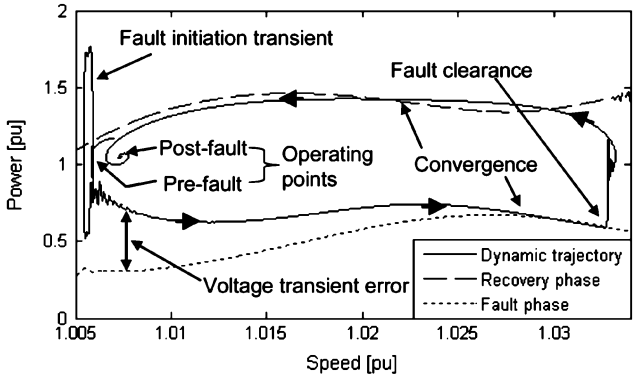

Fig. 17. Correlation of dynamic simulation with quasi-steady-state.

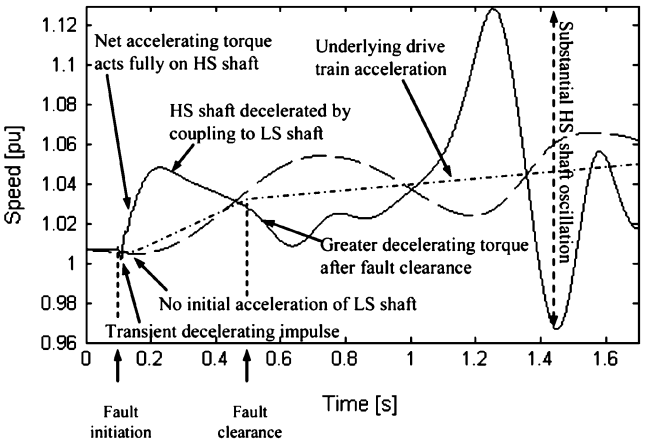

Fig. 18. Speed-time response of wind farm drive train.

and dynamic RPC technologies using a two-mass wind farm model.

The model of Fig. 15 is run with a fault scenario of 384 ms at 30% residual voltage selected from the fault duration profile of Fig. 6. A shorter, deeper voltage dip was selected because this type of fault is typically more severe for two-mass drive trains. This is because destabilizing oscillations are excited in the two-mass system by the large voltage steps associated with the shorter faults. These oscillations are shown in the results of Fig. 18.

Fig. 18 shows the base-case system's dynamic response to the 384-ms fault scenario. After an initial transient decelerating impulse at fault initiation, the step reduction in electrical decelerating torque results in large acceleration of the high-speed (generator rotor) shaft. The relatively low inertia of this shaft means that its acceleration is much larger than observed for a corresponding single mass simulation. The step torque excites two-mass oscillations superimposed on underlying drive train acceleration. Fault clearance imposes a second torque step that excites further oscillation but reduces the underlying acceleration. However, the average decelerating torque during the recovery phase is not sufficient to allow recovery of the system, and the WT would probably trip on overspeed protection during the first positive swing after fault clearance.

Having discussed the fundamental dynamic response of the base-case system, Fig. 19 compares the system response with SDBR and dynamic RPC inserted. The values of SDBR resistance and dynamic RPC capacitance used in the study were

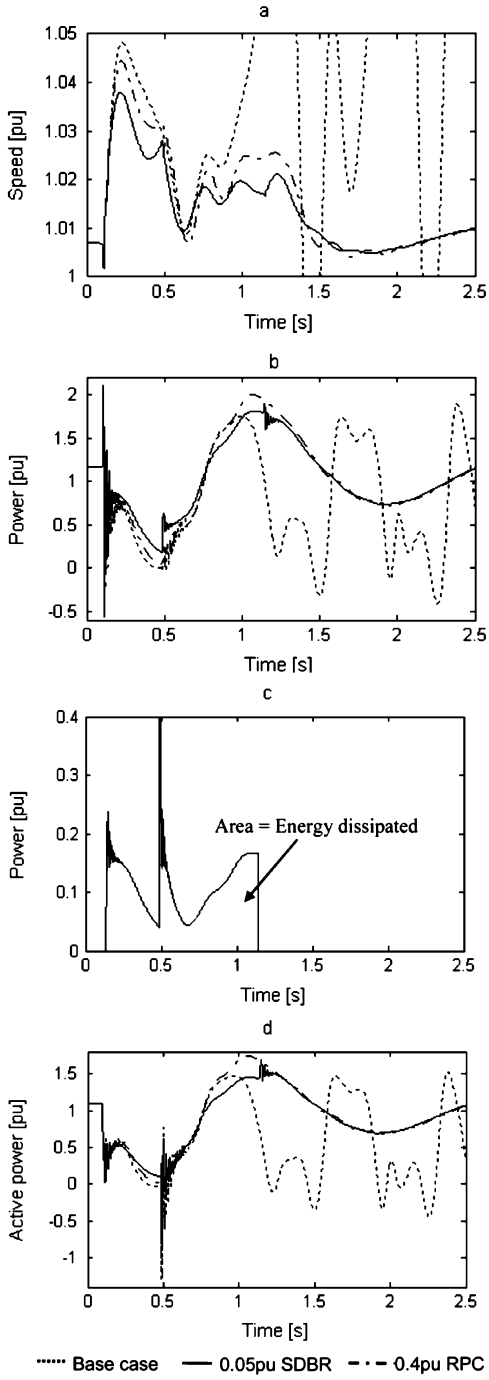

Fig. 19. Effect of SDBR and dynamic RPC on FRT performance. (a) Speed-time curves. (b) Mechanical power-time curves. (c) SDBR power-time curves. (d) Export power-time curves.

selected as the minimum necessary to secure comparable and sufficient stability over the full range of faults defined by the voltage duration profile of Fig. 6.

During the fault, SDBR mitigates acceleration more strongly than dynamic RPC [see Fig. 19(a)]. This effect is a result of the additional power extracted from the mechanical system [see Fig. 19(b)] of which some is exported into the grid [see Fig. 19(d)] and the remainder is dissipated in the SDBR resistor [see Fig. 19(c)].

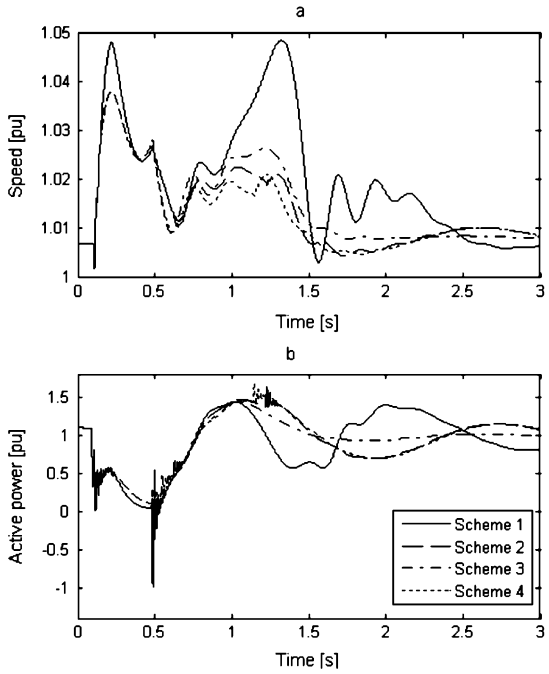

Fig. 20. Sensitivity of SDBR switching times on FRT performance. (a) Speed-time curves. (b) Export power-time curves.

TABLE III
SDBR SWITCHING SCHEMES

Scheme no.	Switch-in (s)	Switch-out (s)
1	0.12	0.52
2	0.12	1.12
3	0.04	0.44
4	0.04	1.04
Note: Time is given w.r.t. fault initiation		

During the recovery, both technologies act similarly to limit post-fault oscillations and give rise to stable operation in about 2.5 ss. In both cases, power export to the grid is restored above 0.9 p.u. within 0.5 s of fault clearance [see Fig. 19(d)], although subsequent oscillations do cause some further reduction below this level.

The energy dissipated by SDBR [see Fig. 19(c)] determines its size and cost. This energy can be optimized by changing the switch-out time. The switch-in time, on the other hand, should always be as short as possible to maximize its speed limitation effect. In this study, SDBR is modeled on the LV system, and therefore, 40 ms has been used as the likely time from fault detection to contactor interruption. In the case of central SDBR, MV switching would give rise to slower insertion times in the order of 120 ms. Fig. 20 compares the four SDBR switching schemes defined in Table III.

It can be observed that scheme 3 has the most stable response and will clearly dissipate significantly less energy in the resistor than scheme 4. The marginal stability of scheme 1 highlights the importance of rapid insertion with centralized SDBR. The energy dissipated in the resistor using the optimum scheme 2 is calculated as 0.05 p.u. This implies that a 2-MW WT would require a resistor thermally rated at 100 kJ for a distributed SDBR scheme. Alternatively, a 40-MW wind farm would require a central resistor thermally rated at 2 MJ.

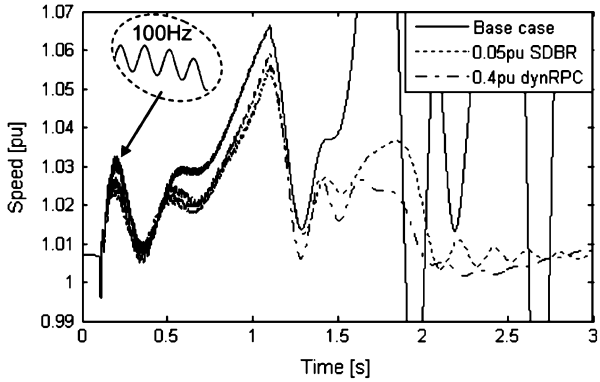

Fig. 21. Effect of SDBR and Dynamic RPC on FRT performance.

D. Unbalanced Simulation

Although the majority of grid faults are unbalanced, grid codes tend to focus on FRT requirements for balanced fault conditions. The assumption is that balanced faults are more onerous for generator stability than unbalanced ones. Although this is generally the case, it is instructive to observe the response of the representative wind farm for a shorted phase-to-phase fault cleared by slow-acting backup protection after one second. The recovery is assumed to be at rated grid voltage.

Fig. 21 shows that this is a very onerous fault that results in instability for the base-case example and marginal stability with each of the FRT technologies. The dynamic RPC actually recovers more rapidly because of the fact that SDBR is switched out only 40 ms after fault clearance (total insertion time of one second). The importance of this scenario is the fact that the energy dissipated in SDBR is higher than the balanced case (0.15 p.u. in the above example). This could therefore become the limiting factor for SDBR thermal design.

VII. CONCLUSION

SDBR has been shown by transient simulation to significantly improve the FRT performance of a representative large wind farm comprising FSWTs. Centralized or distributed SDBR is shown to be capable of transforming an unstable wind farm response into a comfortably stable one without the need for pitch control or dynamic RPC. This improvement is achieved over an extensive range of balanced and unbalanced faults as typically specified by grid codes. Direct comparison of SDBR and dynamic RPC for the representative wind farm concludes that a 0.05-p.u. dynamic resistor is equivalent to 0.4 p.u. of dynamic RPC. As well as a substantial capital cost advantage, SDBR has the potential for higher reliability and lower maintenance.

Quasi-steady-state analysis has been demonstrated in theory and applied as a useful tool for characterizing SDBR performance and predicting transient stability. This method illustrates the extent and limitation of the beneficial effects of SDBR and allows generic comparison with alternatives technologies such as dynamic RPC. It is shown to be particularly useful for assessment of longer faults whether the transient influences are less significant. Quasi-steady-state analysis therefore underpins the results of specific transient studies.

An important design factor for SDBR is its switching regime. A study of the sensitivity of SDBR performance to insertion delay and duration concludes that an optimum scheme would typically achieve rapid insertion and early switching out of the dynamic resistor. Such a scheme can result in rapid stabilization of export power combined with low thermal loading of the resistor.

ACKNOWLEDGMENT

The first author would like to thank A. Wilson of NaREC for his encouragement and support in the course of this project.

REFERENCES

[1] ESB National Grid, *The Grid Code: Version 1.2,* 2005.
[2] E. Fagan, S. Grimes, J. McArdle, P. Smith, and M. Stronge, "Grid code provisions for wind generators in Ireland," in *Proc. IEEE Power Eng. Soc. General Meeting*, 2005, pp. 3073–3079.
[3] A. Johnson and N. Tleis, "The development of grid code requirements for new and renewable forms of generation in Great Britain," presented at the 5th Int. Workshop Large Scale Integration of Wind Power and Transmission Networks for Offshore Wind Farms, Glasgow, U.K., 2005, unpublished.
[4] National Grid Electricity Transmission plc*, The Grid Code*, Revision 17, Issue 3, 2006.
[5] I. Erlich and U. Bachmann, "Grid code requirements concerning connection and operation of wind turbines in Germany," presented at the IEEE Power Eng. Soc. General Meeting, 2005, unpublished.
[6] E. O. Nezt, "Grid code," *High and Extra High Voltage*, 2006.
[7] L. Hansen*, Conceptual Survey of Generators and Power Electronics for Wind Turbines*. Roskilde, Denmark: Risø National Lab., 2001.
[8] A. D. Hansen, , T. Ackermann, Ed., "Generators and power electronics for wind turbines," in *Wind Power in Power Systems*. Chichester, U.K.: Wiley, 2005.
[9] A. Causebrook, "Dynamic Braking of Electric Generators for Fault Ride-through Control," U.K. Patent Application no. GB0526133.4, 2004, Newcastle Univ.
[10] A. Causebrook, D. Atkinson, and A. Jack, "Fault ride-through: shifting the balance of power from blade pitch to electrical resistance," presented at the Eur. Wind Energy Conf., Athens, Greece, 2006, unpublished.
[11] X. Wu, A. Arulampalam, C. Zhan, and N. Jenkins, "Application of a static reactive power compensator (STATCOM) and a dynamic braking resistor (DBR) for the stability enhancement of a large wind farm," *Wind Eng. J.*, vol. 27, pp. 93–106, 2003.
[12] W. Freitas, A. Morelato, and W. Xu, "Improvement of induction generator stability using braking resistors," *IEEE Trans. Power Syst.*, vol. 19, no. 2, pp. 1247–1249, May 2004.
[13] D. F. Peelo, D. W. Hein, and F. Peretti, "Application of a 138 kV 200 MW braking resistor," *Power Eng. J. [See Also Power Engineer]*, vol. 8, pp. 188–192, 1994.
[14] R. Patel, T. S. Bhatti, and D. P. Kothari, "Improvement of power system transient stability by coordinated operation of fast valving and braking resistor," *Proc. Inst. Elect. Eng., Gen., Transm., Distrib.*, vol. 150, no. 3, pp. 311–316, May 2003.
[15] J. Manwell, J. McGowan, and A. Rogers*, Wind Energy Explained*. New York: Wiley, 2002.
[16] H. Knudsen and J. N. Nielsen, , T. Ackermann, Ed., "Introduction to the modeling of wind turbines," in *Wind Power in Power Systems*. Chichester, U.K.: Wiley, 2005.
[17] V. Akhmatov, , T. Ackermann, Ed., "Full-scale verification of dynamic wind turbine models," in *Wind Power in Power Systems*. Chichester, U.K.: Wiley, 2005.
[18] V. Akhmatov and K. Søbrink, "A static VAR compensator model for improved ride-through capability of wind farms," *Wind Eng.*, vol. 28, pp. 715–728, 2004.
[19] V. Akhmatov and K. Søbrink, "Static synchronous compensator (statcom) for dynamic reactive-compensation of wind turbines," *Wind Eng.*, vol. 30, pp. 43–54, 2006.

Andrew Causebrook received the B.Sc. degree in electrical engineering from Imperial College, London, U.K., in 1986 and the M.Sc. degree in renewable energy technology from Loughborough University, Loughborough, U.K., in 1998. He is pursuing the Ph.D. degree on the fault ride-through of wind farms at Newcastle University, Newcastle upon Tyne, U.K.

He has been Principal Engineer with Econnect Ltd., U.K., since 1999, advising clients on the grid integration of wind farms. He was a member of the Scottish Grid Code Review Sub-panel in 2001–2002 that developed early requirements for the connection of wind farms. He formed AC Renewables Limited in 2007, specializing in the grid integration of renewable energy.

Mr. Causebrook is a member of the IET.

David J. Atkinson received the Ph.D. degree from The University of Newcastle upon Tyne, Newcastle upon Tyne, U.K., for research into the use of Kalman filter-based estimation on induction motor vector controlled drives.

He is currently a Senior Lecturer in the Drives and Machines Group at the University of Newcastle. His research interests include electrical drive systems, real-time estimation and control, power electronics, and wind power generation. Current research project involvement includes sensorless vector drives, fault-tolerant drives, and cascade induction generators. Prior to his university appointment in 1987, he had spent 17 years in industry.

Dr. Atkinson is a member of the IET.

Alan G. Jack (M'00) received the Ph.D. degree in 1975 from Southampton University, Southampton, U.K., for work on numerical analysis of electromagnetic fields in turbogenerators.

He is currently with Newcastle University, Newcastle upon Tyne, U.K, where he is the Chair of the Department of Electrical, Electronic, and Computer Engineering, a past head of the department, and leader of the Newcastle Electric Drives and Machines Group. He is the author of over 80 papers in the area of electrical machines and drives. He has been with the university for over 20 years, joining them from NEI Parsons, who he was with for 13 years, with roles from Craft Apprentice to Principal Design Engineer.